

**Influence of B-site transition metal in perovskites on steam  
reforming activity of methane**

Srikanth Dama

Catalysis division

National Chemical Laboratory

PUNE

**Submitted to NCCR**

14th Orientation program

Under guidance of

Dr. C.V.V. Satyanarayana

## Abstract

Steam methane reforming (SMR) is a widely used process in industry for the production of hydrogen, which is considered as the future energy carrier. Recently, there was more focus on hydrogen production for fuel cells, as the later are considered to be the most efficient and the lowest pollutant emission energy sources. Therefore, production of hydrogen from fossil fuels, such as gasoline, natural gas or diesel has become a scientific challenge as the catalysts required should be more efficient and stable under dynamic operating conditions, hence different from those being used by industry. The objective of this review is to report the influence of transition metal containing perovskites in steam reforming reaction and their physicochemical properties. Perovskite-like oxides can be tailored to create a wide family of catalysts, by varying either the A-site or the B-site metal ion, or both. Indeed, the reforming activity of a perovskite can be modified by inserting proper transition metal ions. The main property of perovskites is structural defect. Structural defects are responsible not only for part of the catalytic activity, but also for oxygen mobility within the crystal lattice of the solid due to the non-stoichiometry created by the substitution. The lattice oxygen in perovskites is considered to play important roles in promoting the oxidation of  $\text{CH}_x$  fragments adsorbed on metallic particles and defects are responsible for dissociation of water molecules in the steam reforming reaction. Transition metal containing perovskites are well known as very good reforming catalysts that are cheaper than noble metal supported catalysts. The main effect of impurity on the defect perovskite chemistry of compounds results from their difference in oxidation state relative to the ion they replace and requires the creation of some other defects having the opposite charge to preserve electro neutrality.

## 1. Introduction

Environmental problems, such as air pollution as a result emission of harmful gases into the atmosphere, are being intensely discussed and debated through conferences by researchers as well heads of various governments in order to frame a strict environmental policy to control and limit the emissions. Gases such as NO, N<sub>2</sub>O, CO, CO<sub>2</sub>, CH<sub>4</sub> and SO<sub>x</sub> contribute to the greenhouse gas effect; lead to destruction of the ozone layer. One of the important decisions that emanated out of this concern is minimization of these gas emissions into the atmosphere through the mandatory use of catalytic converters (containing noble metals such as Pd, Pt and Ru) in automotive vehicles, converting some of these harmful gases through combustion or decomposition to CO<sub>2</sub>, H<sub>2</sub>O and N<sub>2</sub><sup>1</sup>. Methane, which is a by-product formed in several industrial processes, and a major hydrocarbon air pollutant received from natural gas fueled vehicles and gas power plants, has a much greater damaging potential as greenhouse gas than carbon dioxide. The inert nature of methane precludes its facile homogeneous oxidative destruction at low temperatures (below 873 K)<sup>2</sup>.

Hydrogen (H<sub>2</sub>) has a long tradition as an energy carrier as well as an important feedstock in chemical industries petroleum refineries. It has the highest energy density (33.3 kWh/kg) compared to any other substance, as it has the same amount of energy as 2.6 kg of natural gas/methane (CH<sub>4</sub>) or 3.1 kg of gasoline. This makes H<sub>2</sub> an ideal fuel in applications where weight rather than volume is an important factor. Hydrogen production has multiple application areas in chemical industry, food industry and fuel cell systems. Due to the major advantages in efficiency and environmental benefits, hydrogen energy in conjunction with fuel cells has attracted considerable attention in the global arena. H<sub>2</sub> production is a major issue in the development of hydrogen based energy systems. Unlike the primary energy sources such as petroleum, coal and natural gas; hydrogen has to be produced from another primary source through chemical transformation. Development of science and technology for H<sub>2</sub> production is also important in the future for more efficient chemical processing and for producing ultraclean fuels. Figure 1 shows worldwide energy distribution<sup>3</sup>.

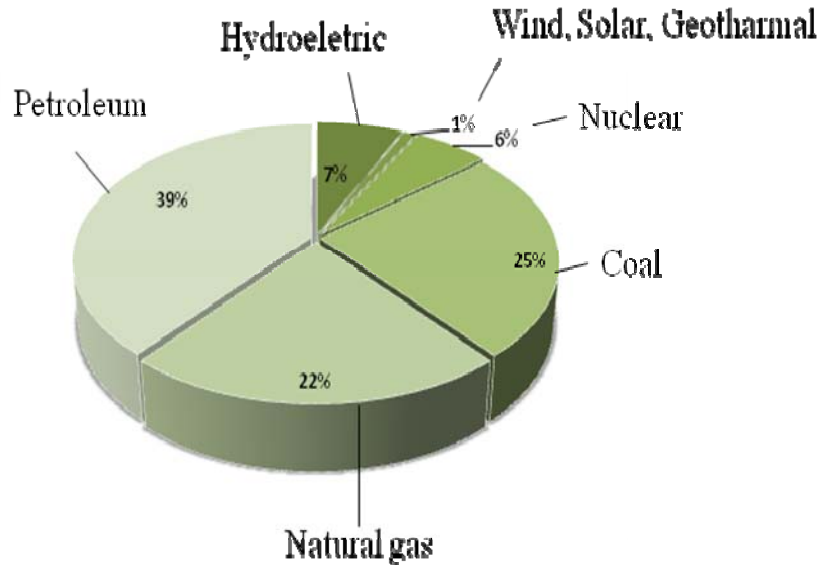


**Fig 1.** World wide energy distribution.<sup>3</sup>

## 2. Steam reforming of methane for the production of hydrogen and syngas

Catalytic steam reforming is the main route to produce hydrogen in petroleum refineries and in ammonia manufacture.

Steam methane reforming (SMR) process involves two main reactions:



The first reaction is reforming, while the second is the water-gas shift reaction. The overall reaction is described as follows:



Since the overall reaction is endothermic, it is necessary to supply the required heat to the reaction by some external means. It is usually accomplished by combustion of a part of the fuel in direct-fired or indirectly fired furnaces. The equilibrium concentrations for reaction (1) are shifted to the right at high temperatures and low pressure. To achieve an almost complete conversion of the methane to CO and H<sub>2</sub>, high temperatures and long residence time is necessary, meaning an overall energy loss and a huge size for the methane reforming reactor. By

using catalysts it is possible to reduce the residence time for total conversion of the methane and tars to below 800 °C at atmosphere pressure.

Methane reacts with steam in the presence of a supported nickel catalyst to produce a mixture of CO and H<sub>2</sub>, also known as synthesis gas or syngas as represented by equation 1. This reaction (SMR) is widely practiced for industrial production of H<sub>2</sub>. However, SMR is not really just one reaction, but involves contributions from several different catalyzed reactions such as water gas shift (WGS, eq.2), reverse water gas shift (RWGS, eq.4), CO disproportionation (Boudouard reaction, eq.5), methane decomposition (eq.6) and carbon gasification (eq.7).

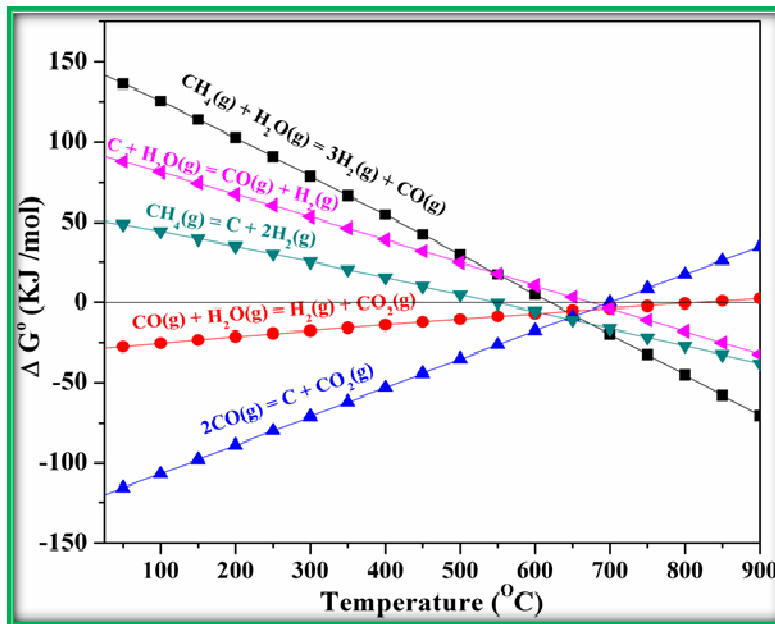
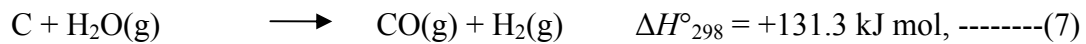
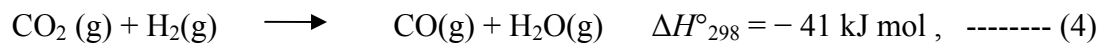


**Fig.2.** Variation of  $\Delta G$  as a function of temperature for steam reforming and other reactions. Generated using the HSC 5.1 Thermochemical calculation software.

Figure 2 shows variation of  $\Delta G$  as a function of temperature for five representative reactions during the SMR process. In SMR, methane decomposition and carbon gasification,  $\Delta G$  declines as temperature increases, reflecting the endothermic nature of those reactions. It can be

seen that methane decomposition, which leads to coke deposition, occurs at relatively low temperature, around 500 °C. However, SMR and carbon gasification reactions require fairly high temperatures (> 700 °C) to move forward. Hence there is a requirement for the development of optimum heat transfer reactor design and optimum catalyst.

Perovskite oxides with the general formula  $ABO_3$  have been tried as catalysts for a large variety of reactions. The ideal perovskite structure is cubic although it may be somewhat distorted according to the type of the A and B cations involved. Typical A elements are rare earths or alkaline earths metals, while the B sites are usually occupied by transition metals. These oxides offer the possibility of preparing a large series of isomorphous solids for the study of the effect of partial substitution of A and B cations ( $A_{1-x}A'_x B_{j-y}B'_y O_3$ ) on catalytic behavior. These oxides are stable at elevated temperatures and may be used in many areas where other formulations fail, e.g., high temperature catalytic combustion,  $CO_2$  reforming and steam reforming.

The first patent on steam methane reforming of natural gas was awarded to BASF in 1926 and the first reforming plant was built in the 1930. Large-scale production started only in the beginning of 1960's following the discovery of large gas fields in Europe and the subsequent changeover from use of coal to natural gas as a feedstock. The modern reforming processes are normally designed to operate at high pressure (~ 25 – 30 bar) and at temperatures around 1000 °C. The reason for the high operation pressure is to save compression energy in the downstream synthesis stage.

Natural gas is purified from impurities such as sulphur, which is a well-known catalyst poison before processing. The product gas from biomass gasification contains a considerable amount of higher hydrocarbons (aliphatic, aromatic). These compounds compete with methane in endothermic reforming reactions, demanding a higher energy input than that calculated for only methane reforming. The high calorific value of the natural gas permits to “burn” a considerable amount of the gas to increase the temperature needed for reforming reactions. The start point for the reaction is a mixture of  $H_2O/CH_4$ , with relatively high steam concentration.

### 3. General characteristics of perovskites as catalysts.

The majority of catalysts used in modern chemical industry are based on mixed metal oxides. The preparation of specific tailor-made mixed oxides able to perform complex functions is one of the main topics of research in the field of heterogeneous catalysis. Achieving complex catalytic reactions requires a polyfunctional catalysts with appropriate solid state structure, surface and morphology. The extensive background knowledge in solid state chemistry may be successfully applied in the design of catalyst and the engineering of new high performance materials. A wide cross-fertilization bridges heterogeneous catalysis and materials science in the fields of physicochemical characterization, solid-state chemistry and routes of synthesis.<sup>4</sup>

Among the mixed metal oxides, perovskite-type oxides remain prominent. The perovskite oxides have the general formula  $ABO_3$  (A cation of larger size than B). Although the most numerous and most interesting compounds with the perovskite structure are oxides crystallized in this structure. This review will focus on the study of B- site transition metal properties and their relevance to steam reforming.<sup>4</sup>

### 4. Structure of Perovskites

#### Crystal Structure

The ideal perovskite structure is cubic with space group  $Pm\bar{3}m(O_h)$ <sup>4,5</sup>. In the unit formula of perovskite-type oxide  $ABO_3$ , A is the larger cation and B is the smaller cation. In this structure, the B cation is 6-fold coordinated and the A cation is 12-fold coordinated with the oxygen anions. Figure 3 depicts the corner sharing octahedra that form the skeleton of the structure, in which the center position is occupied by the A cation. Alternatively, this structure can be viewed with the B cation placed in the center of the octahedron and the A cation is in the center of the cube. The perovskite structure is thus a superstructure with a  $ReO_3$ -type framework built up by the incorporation of A cations into the  $BO_6$  octahedra. The significance and role of the  $ReO_3$ -type framework as a host structure for deriving numerous structures of metal oxides has been emphasized by Raveau.<sup>6</sup>

In the ideal structure, where the atoms are touching one another, the B-O distance is equal to  $a/2$  ( $a$  is the cubic unit cell parameter) while the A-O distance is  $(a/\sqrt{2})$  and the following relationship between the ionic radii holds:  $(r_A + r_O) = \sqrt{2}(r_B + r_O)$ . However, it was found that the cubic structure will still be retained in  $ABO_3$  compounds, even though this equation is not exactly obeyed. As a measure of the deviation from the ideal situation, Goldschmidt<sup>7</sup> introduced a tolerance factor ( $t$ ), defined by the equation :

$$t = (r_A + r_O) / \sqrt{2}(r_B + r_O)$$

which is applicable at room temperature to the empirical ionic radii. Although for an ideal perovskite  $t$  is unity, the  $t$ -values can be in the range of 0.75 to 1.0. The ideal cubic perovskite structure appears in a few cases for  $t$ -values very close to 1 and at high temperatures. In most cases, different distortions of the perovskite structure occurs.<sup>7</sup> Decreasing  $t$  corresponds to an increasing degree of distortion. Correlations between physical properties and the tolerance factor are frequently reported and it has been the tolerance factor largely controls the thermodynamics of perovskites.<sup>8,9</sup> A tolerance factor larger than unity implies that the A cations are too large for the compound to adopt the ideal cubic perovskite structure and in these cases hexagonal perovskites in which octahedra share faces and form chains along the hexagonal  $c$ -axis are often formed.<sup>10</sup>

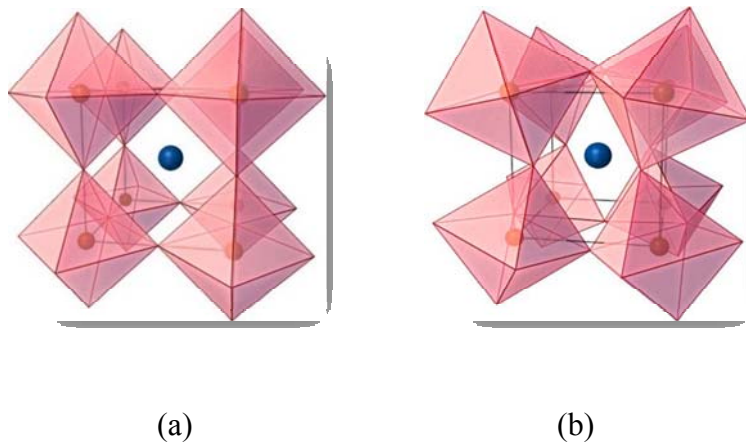


**Fig 3.** (a) cubic perovskite (b) distorted perovskite.

The simple perovskite structure may be appropriately modified by incorporating two types of B ions with different size and charge. The most frequent substitutions are the equiatomic

proportions of the two ions at the B-site, for which the general formula of the perovskite is  $AB_{0.5}B'_{0.5}O_3$ . The resulting unit cell may be viewed as doubled along the three axes, regarding the primitive cell of  $ABO_3$ . If the charge of B and B' is different, in the ordered structure the oxygens are slightly shifted toward the more charged cation although the octahedral symmetry of B and B' cations is still preserved.

The flexibility of the perovskite structure allows not only the incorporation of atoms of widely different sizes but also extended non-stoichiometry. Anion deficient perovskite oxides  $ABO_{3-\delta}$  typically range in composition from  $ABO_3$  to  $ABO_{2.5}$  and the non-stoichiometry results from the reduction of a mixed valence B cation or alternatively from substitution of some B-type cations with cations of a lower oxidation state. At zero degree kelvin, a compound in a true equilibrium state is perfectly ordered. On heating the material, the entropic gain connected with the induction of disorder makes the introduction of defects unavoidable. Thus when considering anion-deficient perovskites  $ABO_{3-\delta}$ , ordered superstructures are often formed at low temperatures while disordered non-stoichiometric phases typically prevail at high temperatures. The formation of superstructures at low temperatures is driven by strong interactions between ions and charged defects giving an enthalpic preference for a certain local environment around a specific cation. While the order–disorder transitions frequently observed in anion-deficient perovskites require several possible local structures of similar energy, extended non-stoichiometry in addition requires that some element can be present in more than one oxidation state. The relative stability of the different oxidation states of the transition metal elements follows general trends that are reflected in the enthalpy of formation of the binary oxides.<sup>10</sup> Data for the first series transition metals are given in Fig. 4.

It is evident that the stability of the trivalent state decreases from iron to nickel (reflected also by the fact that  $Fe_2O_3$  is a stable compound whereas  $Ni_2O_3$  is not). The difference in enthalpy of formation between oxides in different oxidation states is large. This is correct also for ternary oxides although the acid–base arguments considered above imply that the redox

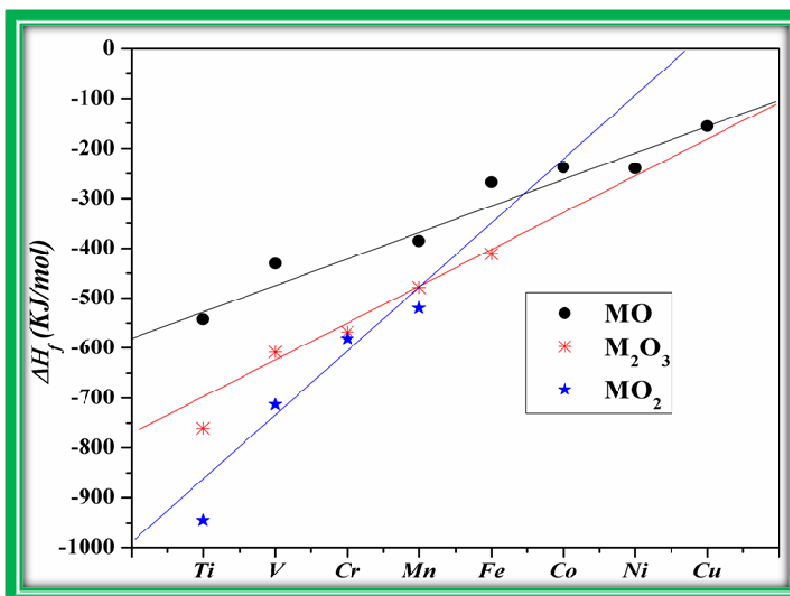


**Fig. 4.** Standard enthalpy of formation (at 0 K) of binary oxides of the first series transition metals.<sup>10</sup> Diagram generated using the HSC 5.1 Thermochemical Calculation software.

energetics of ternary oxides are, in general, quite different from the redox energetics of the binary oxides,<sup>10</sup> while the enthalpy of oxidation of Mn(III)<sub>2</sub>O<sub>3</sub> to Mn(IV)O<sub>2</sub> is  $-158 \text{ kJ mol}^{-1} \text{ O}_2^{-1}$ , the corresponding enthalpies of oxidation (Mn(III) to Mn(IV)) for CaMnO<sub>3- $\delta$</sub>  and SrMnO<sub>3- $\delta$</sub>  are  $-356$  and  $-293 \text{ kJ mol}^{-1} \text{ O}_2^{-1}$  respectively.<sup>11</sup> The enthalpy of oxidation of Fe(III) to Fe(IV) in SrFeO<sub>3- $\delta$</sub>  is large and negative,  $-120 \text{ kJ mol}^{-1} \text{ O}_2^{-1}$ .<sup>12</sup> These coordination geometries are central when considering the evolution of the crystal structure of ABO<sub>3- $\delta$</sub>  during reduction.

## 6. Role of B-site transition metals in steam reforming reaction.

The selection and modification of the catalyst is an effective approach for developing such reforming catalysts. Although improvements of the support greatly impact catalytic activity and/or resistance to coking, limited attempts have been made to use oxygen-ion conducting oxides (for instance perovskite-type oxides) in the steam reforming catalysts. The general stoichiometry of perovskite structure is, ABO<sub>3</sub>, where “A” and “B” are cations and “O” is an anion. Larger size of cation A is responsible for the thermal resistance of the catalyst, while the cation B of smaller size is associated with the catalytic activity. These compounds also offer the possibility to partially substitute B cations by other kinds of cations, thus allowing us to modify

catalytic performance. Full or partial substitution of the A or B cations with cations of different valence is possible. When the overall valence of the A-site and B-site cations ( $n + m$ ) adds up to less than 6, the missing charge is made up by introducing vacancies at the oxygen lattice sites.<sup>13</sup> Recently, a lot of new compounds with perovskite structure have been offered as alternative anode materials in fuel cell application.

Much of the interest in perovskites as reforming catalysts has focused on the ability to suppress carbon deposition, which leads to catalyst deactivation, which is a serious problem with commercial Ni-based steam reforming catalysts.<sup>14</sup> For first row transition metal perovskites, the potential for ensemble size control and strong basicity are two properties that have been suggested as means of suppressing carbon formation when used as catalysts for reforming reactions.<sup>15</sup> Regarding ensemble size control, density functional theory calculations have shown that there is a critical island size required on the surface of Ni particles for graphene formation to occur during reforming.<sup>16</sup> An experimental study done in conjunction with the density-functional theory calculations showed that carbon deposition was suppressed when the Ni particle size of a catalyst is 70 Å as compared to 1020 Å.<sup>16</sup> It has been argued that for ABO<sub>3</sub> perovskite-type oxides, such as La containing first row transition metal perovskites, the B-site cation can undergo reduction but will remain distributed in the structure, resulting in the formation of a well-dispersed metal particle catalyst.<sup>17,18</sup> Regarding strong Lewis basicity, it is known that carbon deposition can be suppressed when Ni is deposited on supports with strong Lewis basicity, which can be achieved by adding an alkaline earth oxide to the support.<sup>19</sup> It is believed that the alkaline earth oxide increases the amount of CO<sub>2</sub> adsorbed on the surface and reduces carbon deposition by the Boudouard reaction ( $2\text{CO} \rightarrow \text{CO}_2 + \text{C}$ ) by shifting the equilibrium towards CO. The lanthanum oxide component is believed to suppress carbon deposition. In fact, several groups have reported that catalysts derived from the perovskite, LaNiO<sub>3</sub> or the perovskite-type structure La<sub>2</sub>NiO<sub>4</sub>, are characterized by a significant resistance to coking.<sup>20-22</sup>

Martinelli et al.<sup>23</sup> reported LaNiO<sub>3</sub> perovskite synthesis using the polymeric precursor method. The results also showed that lanthanum nickelate was more efficient when supported on alumina than zirconia in steam reforming reaction. Figure 5 shows results of methane conversion of the LaNiO<sub>3</sub>, LaNiO<sub>3</sub>/Al<sub>2</sub>O<sub>3</sub> and LaNiO<sub>3</sub>/ZrO<sub>2</sub> catalysts. It was observed that the methane

conversion was approximately 94% and the selectivity to hydrogen was about 70%. In all cases low selectivity to CO and CO<sub>2</sub> was verified.

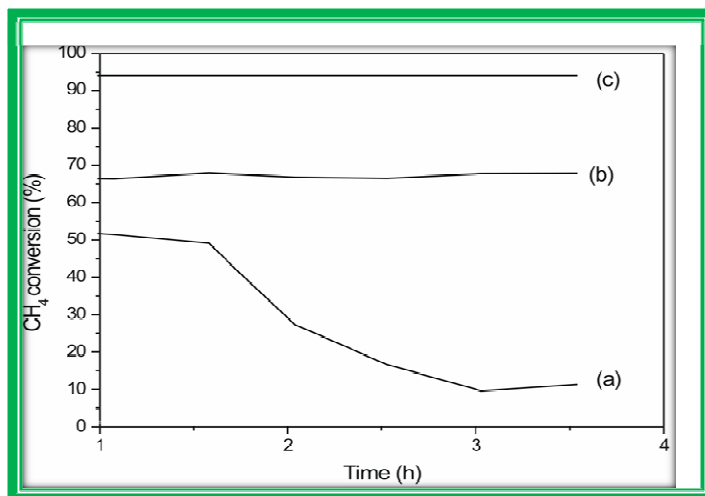


**Fig. 5.** Methane conversion on (a) LaNiO<sub>3</sub>, (b) LaNiO<sub>3</sub>/ZrO<sub>2</sub> and (c) LaNiO<sub>3</sub>/Al<sub>2</sub>O<sub>3</sub>.<sup>23</sup>

Garcia et al.<sup>24</sup> synthesized LaNiO<sub>3</sub> perovskite in the form of highly crystalline phase. After reduction its structure changed, giving rise to well dispersed nickel metallic particles on a lanthanum oxide and hydroxide matrix. A positive influence of the metallic structure in the combined methane reforming reaction with CO<sub>2</sub>-O<sub>2</sub> was observed. The stability of the structured catalyst was higher compared to that observed for mixed oxide catalyst. In addition, no induction period was required for the structured catalyst.

Gallego et al.<sup>25</sup> studied the kinetic behavior of the Ni/La<sub>2</sub>O<sub>3</sub> catalyst obtained from the LaNiO<sub>3</sub> perovskite in the reforming reaction of methane with carbon dioxide as a function of temperature, CH<sub>4</sub> and CO<sub>2</sub> partial pressures. The catalyst showed high resistance towards deactivation by carbon formation under integral reaction conditions. The XRD data (Fig. 6) of the used catalyst after reaction indicates that lanthanum oxycarbonate La<sub>2</sub>O<sub>2</sub>CO<sub>3</sub>, which is the major species formed at the surface, plays an important role in the dry reforming of methane. The partial substitution of La<sup>3+</sup> with Sr<sup>2+</sup> in La<sub>1-x</sub>Sr<sub>x</sub>NiO<sub>3</sub> structure decreases the oxidation state of Ni favoring its reduction and produces material with the spinel type structure, due to the increase in vacancies that facilitates the mobility of the oxygen toward the surface of the solid reported by Valderrama et al.<sup>26</sup> The redox processes on the perovskite structure occur through

intermediary species and they are not reversible, since changes of phases occur forming first  $\text{La}_2\text{Ni}_2\text{O}_5$  at  $420^\circ\text{C}$ ,  $\text{NiO}$  at  $610^\circ\text{C}$  and  $\text{Ni}$ ,  $\text{La}_2\text{O}_3$  at  $690^\circ\text{C}$ , while  $\text{La}_{0.6}\text{Sr}_{0.4}\text{NiO}_3$  becomes  $\text{NiO}$  at  $500^\circ\text{C}$  and when the temperature increases to  $700^\circ\text{C}$  it is reduced completely to  $\text{Ni}$ ,  $\text{La}_2\text{O}_3$  and  $\text{SrO}$ . Before the reaction an important adsorption of  $\text{CO}_2$  occurs, contributing to the formation of  $\text{La}_2\text{O}_2\text{CO}_3$ .

Choudhary et al. prepared cobalt substituted nickel  $\text{LaNiO}_3$  ( $\text{LaNi}_{1-x}\text{Co}_x\text{O}_3$ ;  $x=0.2$  to  $1$ ) that showed good performance in methane steam reforming.<sup>27</sup> By choosing the appropriate perovskite composition, it is possible to combine in one material good oxygen ion conductivity and high activity by nickel catalytic sites.

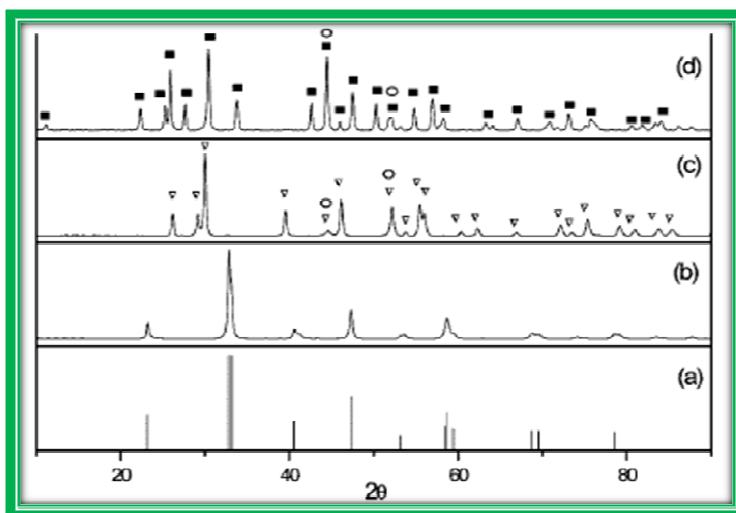


**Fig. 6.** XRD of (a) JCPDF Card No. 88-0633, (b)  $\text{LaNiO}_3$  after calcination for 6 h at  $973\text{ K}$ , (c) after reduction under  $\text{H}_2$  at  $973\text{ K}$ , (d) after 15 h of reaction using the reduced material: (O)  $\text{Ni}$ , (▼)  $\text{La}_2\text{O}_3$ , (■)  $\text{La}_2\text{O}_2\text{CO}_3$  hexagonal.<sup>25</sup>

Provendier et al.<sup>28</sup> synthesized  $\text{LaNi}_x\text{Fe}_{1-x}\text{O}_3$  catalysts, which performed well in syngas production by SMR. The optimum  $\text{H}_2\text{O}:\text{CH}_4$  ratio is 1 for the best yield of hydrogen and CO (93 %) for  $0.2 \leq x \leq 0.8$ . For  $x \geq 0.4$ , the three metal perovskite structures are maintained and a strong interaction between free nickel and the perovskite structure was observed. The Ni metal particle size is lower than obtained with the  $\text{LaNiO}_3$  catalyst thus limiting the coke formation. It also shows good ageing behavior and permits regeneration of the starting structure ( $\text{LaNi}_x\text{Fe}_{1-x}\text{O}_3$ ) after recalcination. The reducing power of the reaction mixture doesn't allow the reduction of the  $\text{LaFeO}_3$  perovskite and therefore no NiFe alloy is formed. For  $x > 0.4$ , only the bimetallic  $\text{LaFeO}_3$

is maintained. Regeneration by calcinations leads to the  $\text{LaNiO}_3$  and  $\text{LaFeO}_3$  perovskites. The increase in the  $\text{H}_2\text{O}:\text{CH}_4$  ratio from 1 to 3 increases the oxidative power of the reaction mixture and leads to a decrease in the activity and enhances the  $\text{CO}_2$  formation. Figure 7 shows variation of Ni content in  $\text{LaFeO}_3$  versus  $\text{CH}_4$  conversion between 600 to 800 °C.

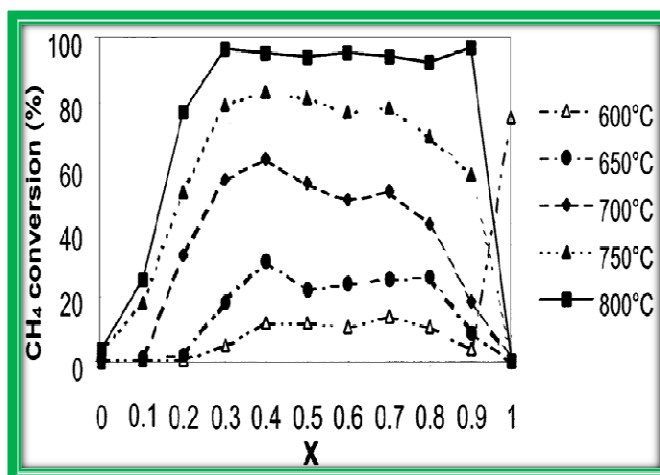


**Fig 7.**  $\text{CH}_4$  conversion versus Ni content (x) on  $\text{LaNi}_x\text{Fe}_{1-x}\text{O}_3$  catalysts ( $600\text{ }^\circ\text{C} < T < 800\text{ }^\circ\text{C}$ ;  $\text{H}_2\text{O}/\text{CH}_4=1$ ;  $\text{CH}_4=1.5\text{ L}\cdot\text{h}^{-1}\cdot\text{g}_{\text{cat}}^{-1}$ ;  $\text{H}_2\text{O}=1.5\text{ L}\cdot\text{h}^{-1}\cdot\text{g}_{\text{cat}}^{-1}$ ;  $\text{Ar}=9\text{ L}\cdot\text{h}^{-1}\cdot\text{g}_{\text{cat}}^{-1}$ ).

Substitution of Ni by Fe was reported by de Lima et al.<sup>29</sup>. It was reported that solid solutions formed at all proportions and a decrease of the area under the first reduction peak (TPR) was observed, indicating that only the Ni was undergoing reduction at this temperature (Fig 8). The temperature of reduction of the second peak increased with the addition of iron, indicating that Ni lean catalysts are more stable under reducing conditions than Ni rich materials.  $\text{LaNiO}_3$  catalysts calcined at 900 °C for 10h presented high initial catalytic activity, but deactivated due to coke formation in dry reforming reaction. Of the substituted catalysts, the  $\text{LaNi}_{0.8}\text{Fe}_{0.2}\text{O}_3$  oxide calcined at 800 °C for 5h was the more active in the reaction conditions, showing that low contents of Fe are sufficient to promote stability for the catalyst. The catalysts calcined at 800 °C were shown to be more active in the reaction conditions than those calcined at 900 °C. Because of the higher values of surface area, the metallic Ni sites exposed on the surface are directly related to the surface area of the catalyst.

During SMR reaction, Ce substituted  $\text{La}_{1-x}\text{Ce}_x\text{Fe}_{0.7}\text{Ni}_{0.3}\text{O}_3$ <sup>30</sup> and  $\text{La}_{0.23}\text{Ce}_{0.1}\text{Sr}_{0.67}\text{TiO}_{3-\delta}$ <sup>31</sup> perovskites were found to show significant resistance to coke deposition with high  $\text{CH}_4$

conversions. It has been suggested that the introduction of Ce to perovskite structures enhanced Ni dispersion and effect of the reduction behaviors of the catalysts. However, the Ce content of  $\text{La}_{1-x}\text{Ce}_x\text{Fe}_{0.7}\text{Ni}_{0.3}\text{O}_3$  was limited to no more than 10%, otherwise the separation of  $\text{CeO}_2$  phase was observed.<sup>30,31,32</sup>

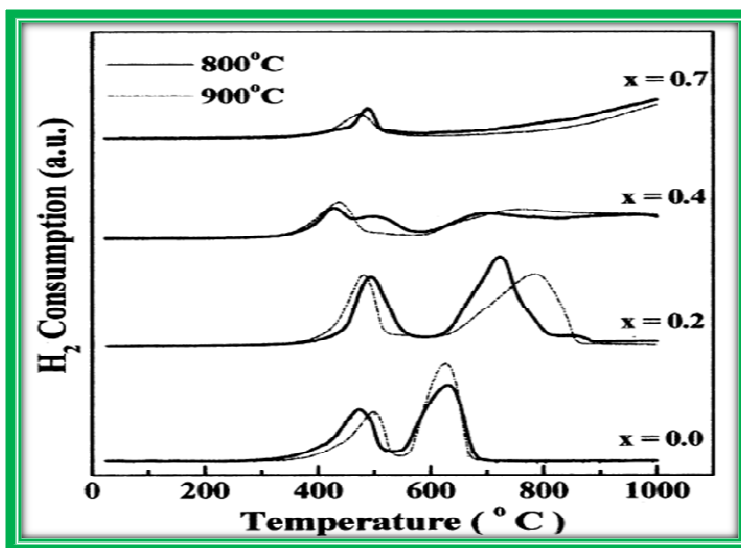


**Fig. 8.** TPR profiles of  $\text{LaNi}_{1-x}\text{Fe}_x\text{O}_3$  perovskite oxides calcined at  $800^\circ\text{C}$  for 5 h and  $900^\circ\text{C}$  for 10 h.<sup>29</sup>

Takehira et al. reported that the perovskite-type oxides such as  $\text{SrTiO}_3$ ,  $\text{CaTiO}_3$ ,  $\text{BaTiO}_3$  that contain a small amount of nickel in the titanium sites show high catalytic activities with high resistance to coking in partial oxidation of methane<sup>33,34,35</sup> and dry reforming of methane<sup>36</sup>, due to the high dispersion of nickel. These researchers also examined oxygen mobility in perovskites, and found that the high resistance to coking might be partly due to the migration of mobile oxygen from the perovskite support to the metallic nickel particles.

The steam reforming of methane employing various Ni containing perovskite catalysts including  $\text{Ni/LaAlO}_3$ ,  $\text{Ni/SrTiO}_3$ ,  $\text{Ni/LaFeO}_3$ ,  $\text{Ni/BaTiO}_3$  and  $\text{Ni/La}_{0.4}\text{Ba}_{0.6}\text{Co}_{0.2}\text{Fe}_{0.8}\text{O}_{3-\delta}$  were studied under the conditions of 1073 K, atmospheric pressure and  $\text{H}_2\text{O}/\text{CH}_4$  ratio of 2 for the purpose of enhancing the catalytic activity to compare conventional  $\text{Ni}/\alpha\text{-Al}_2\text{O}_3$  catalyst and decreasing the coking on the nickel catalyst. The study confirmed that utilization of the lattice oxygen in  $\text{SrTiO}_3$  and  $\text{LaAlO}_3$  effectively promoted the oxidation of  $\text{CH}_x$  fragments adsorbed on metallic nickel reported by K. Urasaki et al.<sup>37</sup>

The beneficial effect of vanadium has been exploited in the development of Sr-doped lanthanum vanadate anodes, which have good sulfur tolerance in solid oxide fuel cell applications.<sup>38,39,40</sup> Vernoux et al.<sup>41</sup> studied catalytic and electrochemical characteristics of  $\text{La}_{0.8}\text{Sr}_{0.2}\text{Cr}_{0.97}\text{V}_{0.03}\text{O}_3$  (LSCV). They found this material exhibited a low activity towards  $\text{CH}_4$  steam reforming at 800 °C, although it has been shown to be stable and does not suffer from carbon deposition. When Ru was added to this electrode to implement the gradual internal reforming process, the LSCV–YSZ composite was a promising anode material.

The introduction of transition elements into the B-site in  $\text{La}_{1-x}\text{Sr}_x\text{Cr}_{1-y}\text{M}_y\text{O}_3$  (M = V, Cr, Mn, Fe, Co, Ni, Cu etc.) has potential for improving the methane reforming properties of such materials. Such improved catalytic effects were reported by Sfeir et al., using 10 mol % transition element doped lanthanum chromite.<sup>42</sup> In a recent report, catalytic properties of  $\text{La}_{0.2}\text{Sr}_{0.8}\text{Cr}_{0.2}\text{Fe}_{0.8}\text{O}_3$  and  $\text{La}_{0.8}\text{Sr}_{0.2}\text{Cr}_{0.2}\text{Fe}_{0.8}\text{O}_3$  for  $\text{CH}_4$ -reforming were investigated.<sup>43-48</sup>

Tao et al.<sup>49</sup> reported an oxygen-deficient perovskite  $\text{La}_{0.75}\text{Sr}_{0.25}\text{Cr}_{0.5}\text{Mn}_{0.5}\text{O}_3$ , with comparable electrochemical performance to that of Ni/YSZ cermets and with good catalytic activity for the electro-oxidation of  $\text{CH}_4$  at high temperatures. Very good performance is achieved for methane oxidation without using excess steam.<sup>50</sup> Bossche et al. observed increase in activity with Mn content, the selectivity toward total oxidation observed at high oxygen lattice stoichiometry for materials with high Cr content.<sup>51,52</sup> Z.Yao et al. also observed Cr doped into  $\text{La}_{0.75}\text{Sr}_{0.25}\text{MnO}_3$  lattice the chemical stability of the oxides increased with increasing Cr doping concentration. When the Cr doping concentration reached 40 mol% or higher, the oxides successfully sustained the perovskite structure even after being exposed to a dry 5% $\text{H}_2$ /Ar atmosphere for 24 h at 900°C. From  $\text{H}_2$ -TPR results the increase of Cr doping amount stabilized Mn at 3+ oxidation state.<sup>53</sup>

To understand the mechanism of the catalytic processes occurring at  $\text{La}_{1-x}\text{Sr}_x\text{Cr}_{0.5}\text{Mn}_{0.5}\text{O}_{3-\delta}$ , the X-ray absorption spectra of samples with  $x = 0.2, 0.25, \text{ and } 0.3$  were investigated, with the XANES as shown in Fig. 9. The situation for Mn is very different with the XANES spectra showing a strong shift on reduction for all compositions, confirming that the Mn species changes in oxidation state on reduction, and further, there are also very significant changes in the

EXAFS spectra for Mn on reduction. These results clearly indicate that oxygen is lost in the coordination environment of Mn on reduction but not in that of Cr. In terms of local coordination, this can be understood if one looks at the two-dimensional representation of the perovskite lattice shown in Fig. 10. where it is only the oxygen atoms between two Mn ions that are lost on reduction. As the amount of oxygen in reduction approaches 0.25 per perovskite unit<sup>54</sup>, this corresponds to reduction in coordination of all the Mn ions in the lattice from 6-fold coordination to 5-fold coordination (i.e., the coordination of Mn changes from octahedral toward square pyramidal). As the Cr coordination environment is dominated by octahedral oxygen coordination, the extent of oxygen reduction implies that the core  $\text{MnO}_5$  units tend to share vacant oxygen sites between pairs of such units. On reduction, the oxygen vacancies formed between two manganese ions in LSCM may act as active centers for oxidation reactions. The redox chemistry of manganese may significantly benefit the formation of intermediates that may accelerate the oxidation process. From this point of view, LSCM is a stabilized manganite because its catalytic properties are close to  $\text{La}_{1-x}\text{Sr}_x\text{MnO}_3$ . The introduction of chromium makes the perovskite lattice stable, which makes it possible to use as an anode material for SOFCs.

Evdou et al. reported<sup>55</sup>  $\text{La}_{1-x}\text{Sr}_x\text{MnO}_3$  ( $x = 0, 0.3, 0.7$ ) are active redox catalysts for the two-step steam reforming of methane towards the production of high purity hydrogen. Oxygen is withdrawn from the material during methane oxidation, after the achievement of a characteristic oxygen deficiency level, the support becomes active for the water-splitting reaction to gaseous hydrogen and lattice oxygen that fills the oxygen vacancies. The activity is proportional to the oxygen vacancy concentration. The maximum deficiency level depends on the strontium content and the reaction temperature. The defect chemistry of  $\text{La}_{1-x}\text{Sr}_x\text{MnO}_{3-\delta}$  perovskites has been extensively studied.<sup>56-59</sup> The replacement of trivalent lanthanum ions by divalent strontium ions leads to the formation of  $\text{Sr}_{\text{La}}$  acceptors, which in consequence, results in a change of the valency of manganese ions from 3+ (base valency of manganese in  $\text{LaMnO}_3$ ) to 4+, in agreement with the lattice-charge neutrality condition requirement. During reduction with methane the tetravalent manganese is reduced to trivalent. Since the  $\text{Mn}^{4+}$  concentration increases with  $\text{Sr}^{2+}$  doping, the required oxygen with draw for completing this reduction (i.e. activation) increases with increasing strontium content. However, the lattice-charge neutrality condition must continue to be preserved and this happens with the creation of oxygen vacancies  $V_o$  that compensate the

Sr<sub>La</sub> acceptors. Finally, the higher the strontium content the higher the concentration of oxygen vacancies accommodated within the material lattice after the Mn<sup>4+</sup>/ Mn<sup>3+</sup> reduction during the activation step.

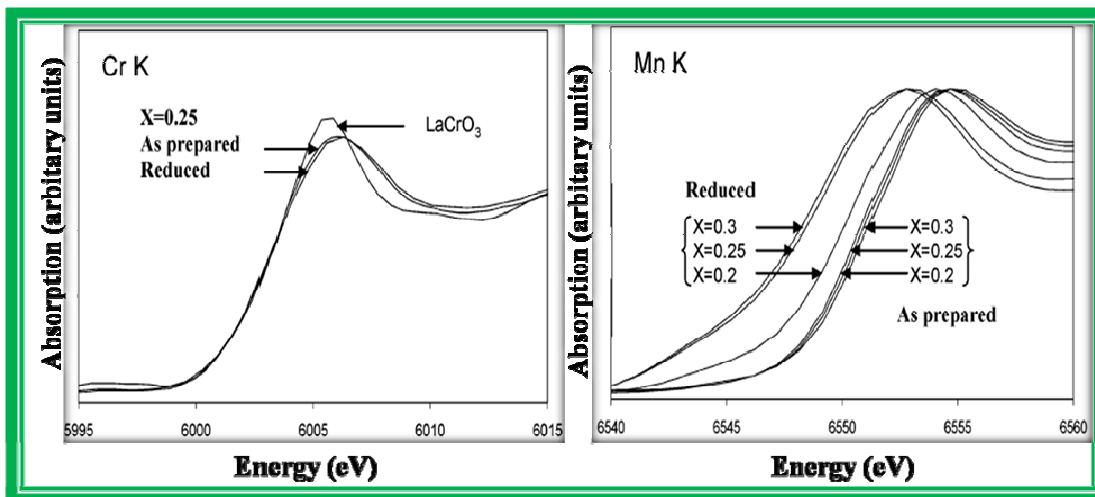


Figure 9. Cr and Mn K XANES spectra for  $\text{La}_{1-x}\text{Sr}_x\text{Mn}_{0.5}\text{Cr}_{0.5}\text{O}_{3-\delta}$ .<sup>55</sup>

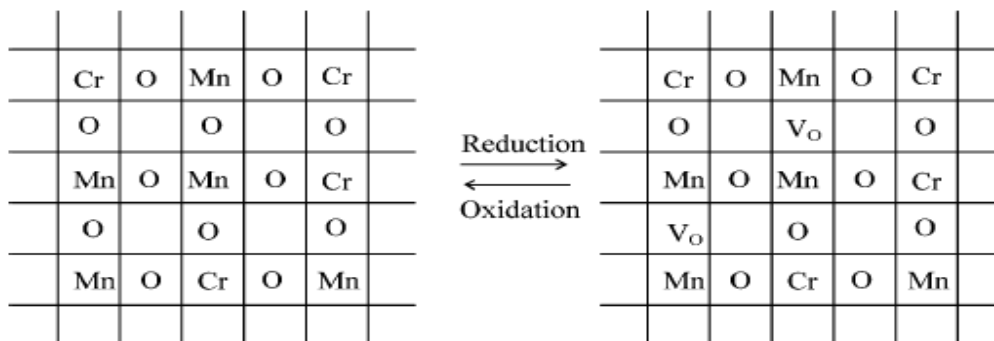


Fig. 10. Formation of oxygen vacancies of  $\text{La}_{1-x}\text{Sr}_x\text{Mn}_{0.5}\text{Cr}_{0.5}\text{O}_{3-\delta}$  in a reducing atmosphere.<sup>55</sup>

Vernoux et al.<sup>60,61</sup> investigated the performances of  $\text{La}(\text{Sr})\text{Cr}(\text{Ru},\text{Mn})\text{O}_{3-\delta}$  defective perovskite materials as an anode material. By inserting ruthenium in the B site, the catalytic activity of this material for the steam reforming of methane has been improved. Catalytic performances are stable, and no carbon deposit was detected, even after 300 h of operation in a reactive mixture containing more methane than steam. It also has shown that the insertion of manganese in the B site accelerates the electrochemical oxidation of hydrogen compared with the strontium-doped lanthanum chromite. It indicated that these perovskite materials are potential

candidates as SOFC anode materials for implementing gradual internal reforming (GIR) of methane. Some literature shows transition metal elements were specifically doped into its B-site with low concentration (3-5 mol%) of dopant, such as  $\text{La}_{1-x}\text{Sr}_x\text{Cr}_{1-y}\text{Ru}_y\text{O}_{3-\delta}$  ( $x = 0.2, 0.3, 0.4$ ;  $y = 0.02, 0.05$ ) (LSCR)<sup>62</sup> and  $\text{La}_{0.8}\text{Sr}_{0.2}\text{Cr}_{0.97}\text{V}_{0.03}\text{O}_3$  (LSCV)<sup>63</sup>, has been investigated. Although LSCR had a high initial catalytic activity, it was not stable in reducing atmosphere due to the depletion of Ru from the lattice to form  $\text{RuO}_2$  oxide phase after a longtime operation.<sup>64</sup> LSCV had a super coking resistant capacity, but polarization resistance was still large under anodic conditions. A higher concentration (~10 mol%) of dopant was introduced into the B-site to form  $\text{La}_{1-x}\text{Sr}_x\text{Cr}_{1-y}\text{M}_y\text{O}_3$  ( $M = \text{Mn, Fe, Co, Ni}$ ) to improve the catalytic properties for methane reforming reaction.<sup>65,66,67</sup>

In the case of  $\text{La}_{1-x}\text{Sr}_x\text{Cr}_{1-y}\text{Ni}_y\text{O}_{3-\delta}$  perovskite incorporation of Ni cations into the lattice of such irreducible perovskites provides a reasonable level of activity in methane steam reforming (Sauvet & Irvine, 2004).<sup>68</sup> Hence, observed high and stable activity of perovskite promoted composites in  $\text{CH}_4$  Steam reforming reaction in stoichiometric feed can be explained by a partial dissolution of NiO in the acidic polyester solution at the preparation stage. At subsequent calcination, Ni-containing perovskite is formed. Under contact with reducing reaction media, small highly reactive Ni clusters are segregated on the surface of perovskite oxide being stabilized by interaction with this matrix stable in reducing conditions. In addition, the surface of big NiO particles in non-reduced composite is covered by the perovskite layers. Hence, big Ni particles generated due to NiO reduction in the reaction media are decorated by perovskite-like oxidic species. A high efficiency of these species and separate perovskite particles in activation of steam and carbon dioxide facilitates gasification of  $\text{CH}_x$  species produced by methane activation on Ni, thus preventing coking.

The surface properties of Fe-based perovskite type oxides with the formula  $\text{La}_{0.6}\text{Sr}_{0.4}\text{Co}_y\text{Fe}_{1-y}\text{O}_{3-\delta}$  for  $y = 0.1, 0.2, \text{ and } 0.3$  were investigated by J. N. Kuhn.<sup>69</sup> The surface basicity, as well as the reducibility, oxygen storage capacity, transition metal surface concentration were found to progress through an extreme for the intermediate Co level, that is, the behavior and performance of the samples are nonlinear with respect to increasing Co content. Hayakawa et al.<sup>70</sup> reported in dry reforming reaction was accelerated when  $\text{Co}^{3+}$  or  $\text{Ni}^{3+}$  in the

perovskite type oxide  $\text{Ca}_{1-x}\text{Sr}_x\text{Ti}_{1-y}\text{M}_y\text{O}_3$  ( $\text{M} = \text{Co}, \text{Ni}$ ) was reduced to the metallic state by the reaction of methane with carbon dioxide.

One of the prominent application of perovskite is good mixed ionic and electronic conducting materials. X. Dong et al. synthesized  $\text{Sr}_{0.7}\text{Ba}_{0.3}\text{Fe}_{0.9}\text{Mo}_{0.1}\text{O}_{3-\delta}$  (SBFM) cubic perovskite oxide was an oxygen-permeable material.<sup>71</sup> This material presented a high reduction-tolerant property and relatively high thermal stability. The high chemical stability of SBFM in a reducing environment was associated with the possible synergistic effect between Mo ion and Fe ion. In addition, SBFM membrane exhibited good oxygen permeability and low oxygen permeation activation energy. The remarkable performances demonstrated that SBFM could be used as an attractive oxygen-permeable material for catalytic membrane reactors.

Zhang et al.<sup>72</sup> Reported Perovskite  $\text{NaCeTi}_2\text{O}_6$  (NCT)-supported Ni catalysts were prepared and examined for the steam reforming of methane (SRM) with a low  $\text{H}_2\text{O}/\text{CH}_4$  ratio (1:1). 4 wt% Ni/NCT catalyst exhibited higher activity than 4 wt% Ni/ $\text{TiO}_2$ , Ni/ $(\text{CeO}_2+\text{TiO}_2)$ , and Ni/ $\text{Ce}_2\text{O}_3$  catalysts for Steam reforming reaction at 973 K, and better resistance to carbon deposition was observed on 4 wt% Ni/NCT compared to 4 wt% Ni/ $\text{CeO}_2$  (Figure.11).

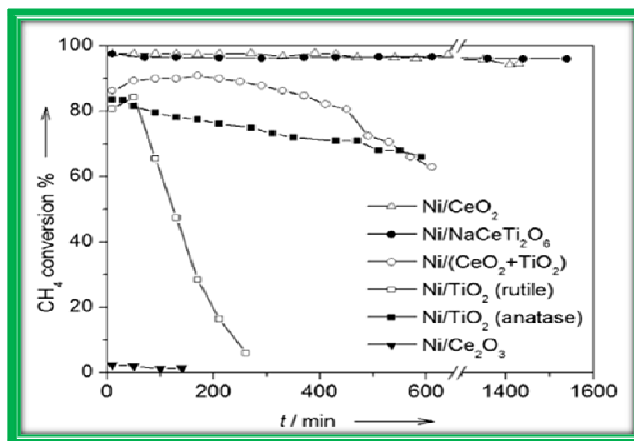


Fig. 11 . Time on stream profiles of the SRM reaction.<sup>72</sup>

It is suggested that the characteristic performance of the Ni/NCT catalysts for the SRM reactions are related to the basic character and oxygen conducting behavior of NCT to control the balance of  $\text{CH}_4$  decomposition and carbon gasification with steam on the surfaces of the Ni/NCT catalysts.

## 7. Conclusions

Mixing together a wide variety of A and B cations on the relevant sublattices promotes ionic transport, strong metal to support interaction. It has been suggested that local structure details are important to understand properties of perovskite systems that show activity in steam/dry reforming reaction. Perovskite like oxides can be tailored to create a wide variety of catalysts, by varying either A-site or B-site metal ion or both. Indeed, the catalytic activity of a perovskite can be modified by inserting proper transition metal ions. Structural defects are responsible not only for catalytic activity, but also for oxygen mobility within the crystal lattice of the solid as a result of the nonstoichiometry created by the substitution. The presence of ionic vacancies effects catalytic activity by favoring reactant adsorption from the gas phase. For instance, an oxygen vacancy in the surface layer is not only the place where oxygen can enter into the solid state structure, but also the site with a missing oxygen ion surrounded by a maximum number of cations represents the more active site, much more active than the regular surface cations.

Catalysis by perovskite type oxides is an emerging research area, which is still awaiting consolidation and rationalization. Much more work is needed before we can form a clear picture of the effects of doping and it's utility. At present, characterization methods are unable to prove beyond doubt that the method of synthesis have yielded a particular transition metal doped perovskite with the dopant imbedded in the surface layer. There is a need to develop new experimental methods that will tell us the morphology and the composition of the surface at an atomic level, under reaction conditions. Because of this, the models used in computations are approximate. To bridge this "model gap", we need to perform calculations of catalysis on surfaces having a variety of "defects" to obtain an estimate of their importance in reactions.

## 8. References

1. Daniele M. H. Martinelli.; Dulce M. A. Melo.; Anne M. Garrido Pedrosa.; Antonio E. Martinelli.; Marcus A. de F. Melo.; Mary K. S. Batista.; Roberto C. Bitencourt., *Materials Sciences and Applications*, **2012**, 3, 363.
2. T.V. Choudhary.; S. Banerjee.; V.R. Choudhary., *Appl.Catal., A* **2002**, 234, 1.
3. K. Liu.; Chunshan Song.; Velu Subramani., *Hydrogen and Syngas Production and Purification Technologies*. John Wiley & Sons: New York, 2010.
4. M. A. Pena.; J. L. G. Fierro., *Chem. Rev.* **2001**, 101, 1981.
5. Moser, W. R., Ed.; *Catalytic Chemistry of Solid State Inorganics*; New York, **1976**.
6. Raveau, B. *Proc. Indian Natl. Sci. Acad.* ,**1986**, 52, 67.
7. Goldschmidt.V. M. ;Skr. Nor. Viedenk Akad.; Kl. I; *Mater. Naturvidensk. Kl.*, **1926**, No. 8.
8. A. Navrotsky., *Physics and Chemistry of Earth Materials*, Cambridge University Press, Cambridge, 1994.
9. S. Støle .; T. Grande., *Chemical Thermodynamics of Materials: Macroscopic and Microscopic Aspects*, John Wiley & Sons: Chichester, 2003.
10. Svein Stølen.; Egil Bakken.; Chris E. Mohn., *Phys. Chem. Chem. Phys.*, **2006**, 8, 429.
11. L. Rørmark.; A. B. Mørch.; K. Wiik.; S. Stølen.; T. Grande., *Chem. Mater.*, **2001**, 13, 4005.
12. L. Rørmark.; S. Stølen.; K. Wiik.; T. Grande., *J. Solid State Chem.* **2002**, 163, 186.
13. B.A. Boukamp., *Nat. Mater.*, **2003**, 2, 294.
14. J.R. Rostrup-Nielsen.; J. Sehested; J.K. Nørskov., *Adv. Catal.* **2002**, 47, 65.
15. D.L. Trimm., *Catal. Today* **1999**, 49, 3.
16. H.S. Bengaard,, *J. Catal.*, **2002**, 209, 365.
17. H. Provendier.; C. Petit, A. Kiennemann., *R. Acad. Sci., Paris, Ser. IIC*, **2001**, 4, 57.

18. J.O. Petunchi, E.A. Lombardo, *Catal. Today*, **1990**, 8, 201–219.
19. T. Horiuchi; Sakuma.K.; Fukui T.; Kubo.Y.; Osaki .T.; Mori.T., *Appl.Catal., A.*, **1996**, 144, 111.
20. J. Guo.; Hui Lou.; Yinghong Zhu.; Xiaoming Zheng.; *Mater. Lett.*, **2003**, 57, 4450.
21. J.W. Nam, A. Parmaliana, Elsevier Science, Amsterdam, **1998**, pp. 843–848.
22. V.R. Choudhary, B.S. Uphade, A.A. Belhekar, *J. Catal.*, **1996**, 163, 312.
23. D. M. H. Martinelli.; D. M. A. Melo.; A. M. Garrido Pedrosa.; A. E. Martinelli.; M. A. de F. Melo.; M. K. S. Batista<sup>1</sup>.; R. C. Bitencourt., *Materials Sciences and Applications*, **2012**, 3, 363.
24. A. Garcia.; N. Becerra.; L. Garcia.; Ini Ojeda.; Estefania Lopez.; Carmen M. Lopez.; M. R. Goldwasser., *Advances in Chemical Engineering and Science*, **2011**, 1, 169.
25. G. Sierra Gallego.; C. B.Dupeyrat.; Joe Barrault.; F. Mondragon.; *Ind. Eng. Chem. Res.* **2008**, 47, 9272.
26. G. Valderrama.; M. R. Goldwasser.; C.Urbina de Navarro.; J. M. Tatibouet.; J. Barrault.; C. B.Dupeyrat.; Fernando Martinez., *Catal. Today.*, **2005**, 107,785.
27. V. R. Choudhary.; B. S. Uphade.; A. A. Belhekar., *J. Catal.*, **1996**, 163,312.
28. H. Provendier.; C. Petit.; Alain Kienneman. *R. Acad. Sci. Paris, Serie IIC*, **2001**, 4, 57.
29. S. M. de Lima.; J. Mansur Assaf., *Catal. Letters.*, **2006**, 108, 1.
30. S. O. Choi.; S. H. Moon., *Catal. Today* **2009**, 146, 148.
31. C. Perillat-Merceroz.; G. Gauthier.; P. Roussel.; M. Huve.; P. Gelin.; R. N. Vannier., *Chem. Mater.* **2011**, 23, 1539.
32. S. M. Lima.; J. M. Assaf.; M. A. Pena.; J. L. G. Fierro., *Appl. Catal. A* **2006**, 311, 94.

33. K. Takehira.; T. Shishido.; M. Kondo., *J. Catal.*, **2002**, 207, 307.
34. K. Takehira.; T. Hayakawa.; H. Harihara.; A.G. Anderse.; K. Suzuki.; M. Shimizu., *Catal. Today.*, **1995**, 24, 237.
35. T. Hayakawa.; H. Harihara.; A.G. Andersen.; K. Suzuki.; H. Yasuda.; T. Tsunoda.; S. Hamakawa.; A.P.E. York.; Y.S. Yoon.; M. Shimizu.; K. Takehira., *Appl. Catal. A.*, **1997**, 149 391.
36. T. Hayakawa.; S. Suzuki.; J. Nakamura.; T. Uchijima.; T. Hamakawa.; K. Suzuki.; T. Shishido.; K. Takehira., *Appl. Catal. A .*, **1999**, 183, 273.
37. Kohei Urasaki.; Yasushi Sekine.; Sho Kawabe.; E. Kikuchi.; M. Matsukata., *Appl Catal. A* **2005**, 183, 23.
38. L. Aguilar.; S. Zha.; S. Li.; J. Winnick.; M. Liu., *Electrochem. Solid-State Lett.* **2004**, 7, 324.
39. S. Li, W. Rauch.; M. Liu.; A. Burke.; J. Winnick., *Electrochem. Soc. Proc.* **2002**, 113.
40. Cheng Peng.; Jingli Luo.; Alan R. Sanger.; Karl T. Chuang., *Chem. Mater.* **2010**, 22, 1032.
41. P. Vernoux.; M. Guilloodo.; J. Fouletier.; A. Hammou., *Solid State Ionics* **2000**, 135, 425.
42. Sfeir, J.; Buffat, P. A.; Mo'ckli, P.; Xanthopoulos, N.; Vasquez, R.; Mathieu, H. J.; Van herle, J.; Thampi, K. R., *J. Catal.* **2001**, 202, 229.
43. Ramirez-Cabrera, E.; Atkinson, A.; Rudkin, R.; Chadwick, D. I. *In Proceedings of the 5th European Solid Oxide Fuel Cell Forum; Huijismans, J., Ed.; Switzerland, 2002*; p 546.
44. Aguiar, P.; Ramirez-Cabrera, E.; Laosiripojana, N.; Atkinson, A.; Kershenbaum, L. S.; Chadwick, D., *Stud. Surf. Sci. Catal.* **2003**, 145, 387.
45. Vernoux, P.; Guindet, J.; Kleitz, M., *J. Electrochem. Soc.* **1998**, 145, 3487.

46. Nakamura, T.; Petzow, G.; Gauckler, L., *J. Mater. Res. Bull.* **1979**, *14*, 649.
47. Yokokawa.; H.; Sakai.; N.; Kawada.T.; Dokiya. M., *Solid State Ionics* **1992**, *52*, 43.
48. Sauvet. A.L.; Fouletier. J., *J. Power Sources* **2001**, *101*, 259.
49. S.W. Tao.; J.T.S. Irvine., *Nat. Mater.* **2003**, *2*, 320.
50. S.W. Zha.; P. Tsang.; Z. Cheng.; Z. Cheng.; M.L. Liu., *J. Solid State Chem.* **2005**, *178*, 1844.
51. M. van den Bossche.; S. McIntosh., *J. Catal.* **2008**, *255*, 313.
52. Shanwen Tao.; J. T. S. Irvine.; Steven M. Plint., *J. Phys. Chem. B* **2006**, *110*, 21771.
53. Zheng Yao.; Ran Ran.; Shao Zongping., *Rare metals* **2009**, *28*, 361.
54. Tao. S. W.; Irvine, J. T. S., *J. Electrochem. Soc.* **2004**, *151*, 252.
55. A. Evdou.; V. Zaspalis.; L. Nalbandian., *Int. J. Hydrogen Energ.* **2008**, *33*, 5554.
56. Roosmalen JAM.; Cordfunke EHP., *J. Solid State Chem.* **1994**, *110*,109.
57. Mizusaki .J.; Mori .N.; Takai .H.; Yonemura .Y.; Minamiue .H; Tagawa .H., *Solid State Ionics* **2000**;129,163.
58. Nakamura .K.; Ogawa K., *J. Solid State Chem.* **2002**, *163*, 65.
59. Nakamura .K., *J. Solid State Chem.* **2003**,173, 299.
60. P. Vernoux.; E. Djurado.; M. Guillodo., *J. Am. Ceram. Soc.* **2001**, *84*, 2289.
61. P. Vernoux.; M. Guillodo.; J. Fouletier.; A. Hammou., *Solid State Ionics* **2000**, *135*, 425.
62. Sauvet .A.L.; Fouletier ., *J. Electrochim. Acta*, **2001**, *47*, 987.
63. Vernoux .P.; Guillodo .M.; Fouletier .J.; Hammou .A., *Solid State Ionics* **2000**, *135*, 425.

64. Sauvet .A.L.; Fouletier .J.; Gaillard .F.; Primet .M., *J. Catal.* **2002**, *209*, 25.
65. Sfeir .J.; Buffat .P.A.; Mockli .P.; Xanthopoulos .N.; Vasquez .R.; Mathieu .H.J.; Van herle .J., Thampi .K.R., *J. Catal.* **2001**, *202*, 229.
66. M. Watanabe.; H. Uchida.; M. Shibata.; N. Mochizuki.; K. Amikure., *J. Electrochem. Soc.* **1994**, *141*, 342,.
67. P.Vernoux.; E. Djurado.; Michael Guillodo., *J. Am. Ceram. Soc.*,**2001**, *84*, 2289.
68. Sauvet, A.L.; Irvine., *J. Solid State Ionics*, **2004**, *167*, 1.
69. J.N. Kuhn.; U.S. Ozkan., *J. Catal*, **2008**, *253*,200.
70. Hayakawa. T.; Andersen .A.G.; Shimizu M., *Catal Lett*, **1993**, *22*, 307.
71. X. Dong.; W. Jin.; Nanping Xu., *Chem. Mater*, **2010**, *22*, 3610.
72. S. Zhang.; S. Muratsugu.; N. Ishiguro.; S. Ohkoshi.; Mizuki Tada, *Chem Cat Chem.*, **2012**, *4*, 1783.